#### RESEARCH



# Geochemistry and formation of agate-bearing lithophysae in Lower Permian volcanics of the NW-Saxonian Basin (Germany)

Jens Götze<sup>1</sup> · Robert Möckel<sup>2</sup> · Yuanming Pan<sup>3</sup> · Axel Müller<sup>4,5</sup>

Received: 15 February 2023 / Accepted: 26 June 2023 / Published online: 22 August 2023 © The Author(s) 2023

#### Abstract

Geochemical and mineralogical investigations of the Lower Permian Kemmlitz rhyolite within the NW-Saxonian Basin (Germany) and associated lithophysae (high-temperature crystallization domains) as well as agates were carried out to constrain the genesis and characteristics of these volcanic rocks and the origin of the agate-bearing lithophysae. The volcanic rocks of rhyolitic composition are dominated by quartz, sanidine, and orthoclase and most likely derive from lava flows. Agate-bearing lithophysae were exclusively formed in a glassy facies (pitchstone) of the rhyolites, which was afterwards altered to illite-smectite mixed-layer clays. The results of this study show that agate formation can be related to the alteration of the volcanic rocks accompanied by the infill of mobilized silica into cavities of lithophysae. Fluid inclusion studies point to temperatures of agate formation above 150 °C, indicating that the mobilization and accumulation of silica started already during a late phase of or soon after the volcanic activities. Remarkable high concentrations of B (29 ppm), Ge (> 18 ppm), and U (> 19 ppm) as well as chondrite-normalized rare earth element (REE) distribution patterns of the agates with pronounced negative Eu-anomalies, slightly positive Ce-anomalies and enriched heavy rare earth elements (HREE) indicate interactions of the host rocks and transport of SiO<sub>2</sub> with magmatic volatiles (F/Cl, CO<sub>2</sub>) and heated meteoric water. Characteristic yellow cathodoluminescence (CL), heterogeneous internal textures as well as high defect density of micro- and macrocrystalline quartz detected by electron paramagnetic resonance (EPR) spectroscopy point to crystallization processes via an amorphous silica precursor under non-equilibrium conditions.

 $\textbf{Keywords} \ \ Permian \ rhyolites \cdot Lithophysae \cdot Agate \cdot Quartz \cdot Geochemistry$ 

#### Introduction

The NW-Saxonian basin (or NW-Saxonian Volcanic Complex) in the north-eastern part of Germany (Fig. 1) hosts one of the largest acidic to intermediate volcanic complexes

Editorial handling: N. Chukanov

- ☐ Jens Götze jens.goetze@mineral.tu-freiberg.de
- <sup>1</sup> Institute of Mineralogy, TU Bergakademie Freiberg, Brennhausgasse 14, 09599 Freiberg, Germany
- Helmholtz-Zentrum Dresden-Rossendorf, Hemholtz Institute Freiberg for Resource Technology, Chemnitzer Str. 40, 09599 Freiberg, Germany
- Department of Geological Sciences, University of Saskatchewan, Saskatoon, SK S7N 5E2, Canada
- <sup>4</sup> Natural History Museum, University of Oslo, Blindern, P.O. Box 1172, 0318 Oslo, Norway
- Natural History Museum, Cromwell Road, London SW7 5BD, U.K.

of Permian age in Europe (Breitkreuz 2016). Numerous geological and petrographical investigations during the last decades provided comprehensive information concerning the genesis and stratigraphic position of these volcanic rocks (e.g., Pietzsch 1962; Hohl and Wilsdorf 1966; Röllig et al. 1970; Röllig 1976; Eigenfeld 1978; Glässer 1983; Wetzel et al. 1995; Walter et al. 1996; Walter 2012; Breitkreuz 2016; Repstock et al. 2018; Götze et al. 2017, 2020a). According to these data, the Permian volcanic rocks (e.g. rhyolitic lava flows and ignimbrites) and associated sedimentary intercalations in the NW-Saxonian Basin can be subdivided into four main formations (from oldest to youngest): Kohren formation, Rochlitz formation, Oschatz formation, and Wurzen formation (Walter 2012).

The ignimbrites of the Rochlitz formation (ca. 295 Ma) as well as the giant caldera system of the Wurzen formation (ca. 289 Ma) are the prevailing rock types and volcanic structures, respectively, of the NW-Saxonian Complex (Röllig et al. 1970; Hoffmann et al. 2013; Repstock et al. 2018). In addition, various lava flows occur in the southern and eastern part of the basin. These lava flows can be assigned to older,



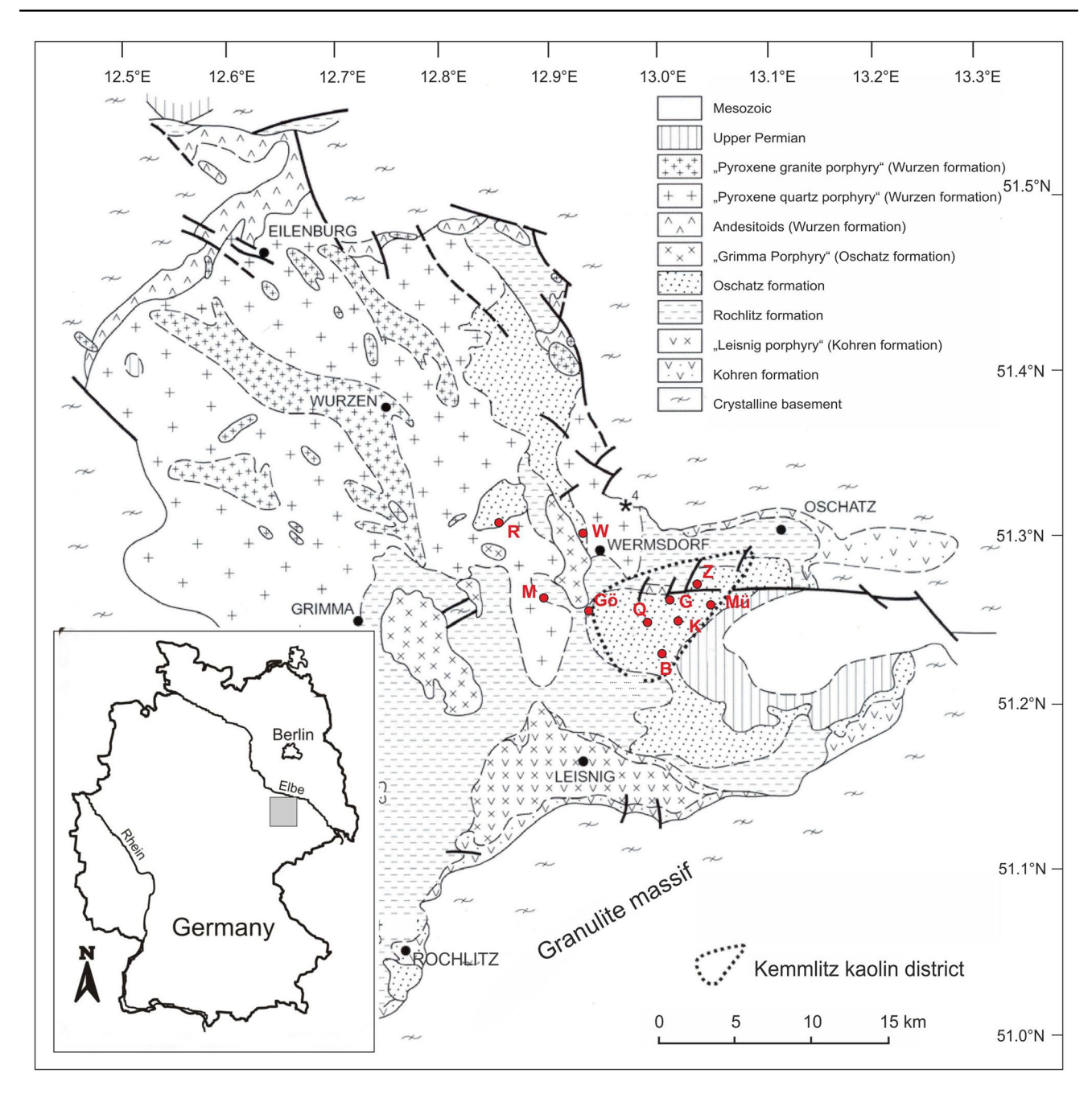


**Fig. 1** Geological map (simplified) showing the NW-Saxonian Basin with the distribution of the different stratigraphic units (modified after Walter 2012). The investigated samples belong to the Kemmlitz rhyo-

lite within the Oschatz Formation: B – Börtewitz, G – Gröppendorf, Gö – Göttwitz, K – Kemmlitz, M – Mutzschen, Mü – Mügeln, Q – Querbitzsch, R – Roda, W – Wermsdorf, Z – Zetzschlig

preignimbritic lavas of the Kohren formation and younger, postignimbritic lavas of the Oschatz formation, which directly overly the Rochlitz ignimbrite (Walter 2012). Our study focuses on the Kemmlitz rhyolite (or "Kemmlitz porphyry" in older geological maps), which belongs to the postignimbritic lavas of the Oschatz formation and occurs in the north-eastern part of the basin (Fig. 1).

The sequence of the Kemmlitz rhyolite is characterized by strong kaolinization, which resulted in the formation of economic kaolin deposits (Schwerdtner et al. 2007). The alteration of the primary volcanic host rocks hinders their petrographic characterization and results in the lack of detailed mineralogical and geochemical data of the Kemmlitz rhyolite. Another conspicuous feature of the Kemmlitz rhyolite is the local occurrence of lithophysae (high-temperature crystallization domains – HTCD), which are formed as spherical aggregates in  $SiO_2$ -rich volcanic melts above the glass transition temperature  $T_g$  (Breitkreuz



2013). Several factors such as shear stress, degassing and/ or corrosion result in the formation of cavities within the lithophysae, which might be filled with secondary mineralization (e.g. SiO<sub>2</sub> – agate, chalcedony). Because of the higher weathering resistance compared to the volcanic matrix, these lithophysae are often preserved, even in areas with strong alteration and kaolinization. Therefore, they can provide valuable information concerning the mineralogy and geochemistry of the primary host rocks.

In this study, we performed an integrated mineralogical and geochemical approach to characterize agate-bearing lithophysae from different locations within the Kemmlitz rhyolite unit. The data are compared with those of the lithophysae-free, massive volcanic type rock aiming the improvement of understanding of the formation of the rhyolites and the associated lithophysae. Finally, the results of the mineralogical and geochemical studies of the associated agates are discussed in terms of processes and conditions of alteration, secondary mineralization, and the origin of the agates.

# **Geological setting**

The Permian rocks of the NW-Saxonian Volcanic Complex have been subdivided into four main formations (Fig. 1; Walter 2012). The 150–200 m thick *Kohren formation* represents the basis of the complex and consists of cyclic sequences of sedimentary silt- and sandstones, which are interlocked with acidic to basic volcanic rocks and pyroclastites. The lava complex of the Leisnig porphyry (298.3 ± 9.1 Ma; zircon SHRIMP U/Pb ages; Hoffmann et al. 2013) is the dominating volcanic unit of the Kohren formation. Based on recent results, Rehda (2018) supposed that the Leisnig porphyry represents a laccolith, which was formed due to the insertion of porphyric acidic lavas into tuff layers of the Rochlitz formation. Such a scenario would result in a younger age of the Leisnig porphyry, probably coeval with the Oschatz formation.

The *Rochlitz formation* with the 400 m thick Rochlitz ignimbrite has the largest regional distribution and, therefore, represents an important stratigraphic unit (Eigenfeld 1978; Walter 2012). The ignimbrite complex consists of four subunits and was dated with  $294.4 \pm 1.8$  Ma by SHRIMP U/Pb analyses on zircon (Hoffmann et al. 2013).

The 150–250 m thick *Oschatz formation* at the NE margin of the basin is built up of alluvial fans and fluvial sediments, which are intercalated by rhyolitic lava flows. These volcano-sedimentary units have an age of  $289.8 \pm 1.9$  Ma (Gold 2011). One of these lava flows formed the Kemmlitz rhyolite, situated between Döbeln–Mügeln–Oschatz covering an area of ca.  $80 \text{ km}^2$  (Eigenfeld 1978; Fig. 1).

A conspicuous feature of the investigated volcanic rocks in the distribution area of the Kemmlitz rhyolite is their strong surficial weathering. The Kemmlitz kaolin district that covers parts of the distribution area (compare Fig. 1) was formed by chemical weathering of the quartz- and feldspar-rich rhyolites during Upper Cretaceous to Miocene periods (Gilg et al. 2003). The 10–40 m thick weathering crust is dominated by kaolinite with minor halloysite and variable amounts of illite-montmorillonite mixed-layer clays (Schwerdtner et al. 2007).

The Wurzen formation with ages of 289.3±4.1 Ma (porphyritic dyke; Hoffmann et al. 2013) and 287.3±3.0 Ma (pyroxene porphyry; Wendt et al. 1995) determined by combined use of U-Pb and Sm-Nd zircon dating as well as Sm-Nd and Rb-Sr whole-rock and mineral systematics is the youngest unit of the Permian sequence and mainly consists of ignimbrites and intrusive rocks. The volcanic rocks probably originate from magma mixing processes and cover an area of ca. 600 km² in the northern part of the basin between Wermsdorf–Eilenburg–Leipzig (Repstock et al. 2018). These rocks are covered by Upper Permian conglomerates and sandstones, as well as locally by Lower Triassic, Oligocene to Miocene and Quaternary sediments.

#### **Materials and methods**

### Sample material

In the present study samples of 10 localities within the Kemmlitz rhyolite were investigated (see Figs. 1 and 2), i.e. one sample of the type rock of the massive, lithophysae-free porphyritic Kemmlitz rhyolite from the socalled Am Zetschlig outcrop (Walter et al. 1996) as well as additional samples from nine occurrences of agate-bearing lithophysae in the distribution area of the Kemmlitz rhyolite (Table 1). The latter material includes four locations that are situated in the area of recent or previous kaolin deposits (Gröppendorf, Kemmlitz, Querbitzsch, Börtewitz) and five further locations (Göttwitz, Mutzschen, Mügeln, Roda, Wermsdorf). Most of the lithophysae occurred either in the loose soil or in a clayey matrix of completely altered host rocks. Therefore, no material of the primary rhyolites formerly hosting the lithophysae was available. If available, the surrounding clay material was sampled for further analytical studies.

# **Analytical methods**

The collected sample material was documented and macroscopically described. Several agate-bearing lithophysae were cut and polished to better visualize the agate textures. Selected aliquots of representative samples from the ten



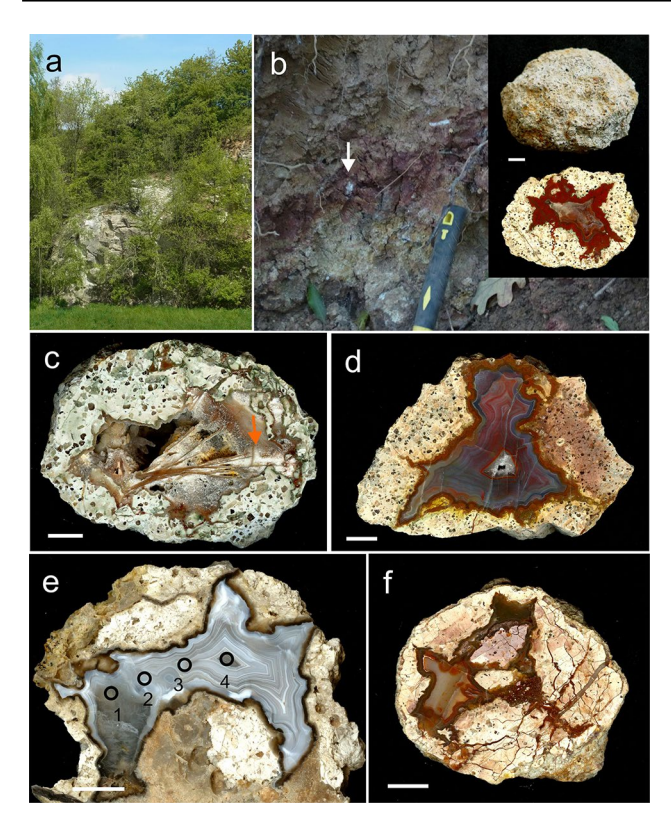


**Fig. 2** Rocks and representative agate samples from the investigated Kemmlitz rhyolite, NW Saxony (Germany); **a** Outcrop of the lithophysae-free porphyritic Kemmlitz rhyolite from the core zone near Zetzschlig; **b** clayey horizon of strongly altered Kemmlitz rhyolite near Mügeln containing agate-bearing lithophysae (arrow); the inset shows a lithophysa from Mügeln before and after cutting; **c** agate in a lithophysa from the kaolin deposit Querbitzsch with lath-shaped pseudomorphs of quartz (after barite and/or bladed calcite/dolmite) in the cavity and white kaolinite in the interstices (arrow); **d** strongly coloured and banded agate from Börtewitz; **e** agate from the kaolin deposit Gröppendorf; the circles and numbers relate to the positions of LA-ICP-MS trace-element analyses (compare Table 5); **f** agate-bearing lithophysa from Mutzschen (scale bar=1 cm)

locations were prepared for further investigations. Polished thin sections (30  $\mu$ m thick) of host rocks, lithophysae and agates were made for microscopic investigations by polarizing microscopy (Polmi), (CL) microscopy and scanning electron microscopy (SEM).

The geochemistry and mineral composition of the volcanic rocks, lithophysae, and surrounding clay matrix were characterized by a combination of X-ray fluorescence (XRF) and powder X-ray diffraction (XRD) analyses on selected and prepared ( $<20~\mu m$ ) sample material. During preparation of the rock samples it was tried to make sure that only fresh material without macroscopically visible secondary mineralization was selected. For XRF measurements, the powdered samples were calcinated, mixed and homogenized with Li-borate (at a ratio of 1:8), and a fusion disc produced. The discs were analyzed using a PANalytical

Axios Minerals spectrometer and WROXI (wide range oxides, PANalytical) calibration.

Qualitative and quantitative phase analyses were made using a PANalytical Empyrean diffractometer, equipped with a Co-tube (Fe-filter), a PIXcel3D medipix detector. The irradiated area was kept constant at  $15 \times 12 \text{ mm}^2$  by the use of an automatic divergence slit. Measurements were done in the 2theta range of 5-80°, with a step size of 0.031 and total measurement time of 2h30min per sample. Data evaluation was realized using the pdf4+database (International Centre for Diffraction Data, ICDD) and the BGMN/Profex v.4.1.0 software package (Doebelin and Kleeberg 2015). In addition, altered clayey material was analyzed using an URD 6 (Seifert/Freiberger Präzisionsmechanik) with Co  $K\alpha$ -radiation in the range 5–80° (2θ). Analytical conditions included a detector slit of 0.25 mm, 0.03° step width and 5 s measuring time. Data evaluation was realized using Analyse RayfleX v.2.352 software and subsequent Rietveld refinement with Autoquan v.2.7.00 according to Taut et al. (1998).

Conventional polarizing microscopy used a Zeiss Axio Imager A1m microscope for petrographic characterization of the rock fabric, texture, phase composition and inclusions in macrocrystalline quartz. These investigations were complemented by SEM measurements (secondary electrons – SE, back-scattered electrons – BSE) using a JEOL JSM-7001F (20 kV, 2.64 nA) with a BRUKER Quantax 800 EDX system. CL measurements were made on carboncoated, polished thin sections using a "hot cathode" CL microscope HC1-LM (Neuser et al. 1995). The system was operated at 14 kV accelerating voltage and a current of 0.2 mA with a Peltier-cooled digital video camera (OLYM-PUS DP72) and an Acton Research SP-2356 digital triplegrating spectrograph with a Princeton Spec-10 chargecoupled device (CCD) detector, respectively. CL spectra in the wavelength range 380 to 900 nm were measured under standardized conditions (wavelength calibration by a Hg-halogen lamp, spot width 30 μm, measuring time 5 s).

The paramagnetic centres of powder agate samples were analyzed by EPR spectroscopy using a Bruker EMX spectrometer. The equipment operated with microwave frequencies of ~9.63 GHz and 9.39 GHz at 295 K and 85 K, respectively. Experimental conditions included modulation frequency of 100 kHz, modulation amplitude of 0.1 mT, and microwave powers from 0.2 to 20 mW to obtain optimal conditions for different centre types. The spectral resolutions were ~0.146 mT for wide scans from 50 to 650 mT and 0.024 mT for narrow scans from 300 to 350 mT.

Trace-element analyses were done by both solution inductively coupled plasma mass spectrometry (ICP-MS) and laser ablation ICP-MS (LA-ICP-MS). The samples (400–500 mg) for solution ICP-MS analysis were milled to a grain size of < 30  $\mu$ m using a pre-cleaned agate mortar. The powdered sample was digested in a glassy carbon vessel



Table 1 Investigated samples from different occurrences in the distribution area of the Kemmlitz rhyolite (NW-Saxonian Basin, Germany) and applied analytics

Location	Sample type	Analytics		
Börtewitz	Lithophysae/agates/altered host rock (clay)	XRF, XRD, Polmi, CL, SEM, ICP-MS,		
		FI, EPR		
Göttwitz	Lithophysae	XRF, XRD, Polmi, CL		
Gröppendorf	Lithophysae/agates/ altered host rock (clay)	XRF, XRD, Polmi, CL, SEM, ICP-MS,		
		LA-ICP-MS, FI, EPR		
Kemmlitz	Lithophysae/agates/ altered host rock (clay)	XRF, XRD, Polmi, CL, SEM		
Mügeln Lithophysae/agates/ altered host rock (clay)		XRF, XRD, Polmi, CL, SEM, ICP-MS,		
		FI, EPR		
Mutzschen	Lithophysae/agates	XRF, XRD, Polmi, CL		
Querbitzsch	Lithophysae/agates/ altered host rock (clay)	XRF, XRD, Polmi, CL, SEM		
Roda	Lithophysae	XRF, XRD, Polmi, CL		
Wermsdorf	Lithophysae	XRF, XRD, Polmi, CL		
Zetzschlig	Massive rhyolite	XRF, XRD, Polmi, CL		

XRF X-ray fluorescence; XRD X-ray diffraction, Polmi polarizing microscopy, CL cathodoluminescence microscopy and spectroscopy, SEM scanning electron microscopy, ICP-MS inductively coupled plasma mass spectrometry, LA-ICP-MS laser ablation ICP-MS, FI fluid inclusion studies (agates), EPR electron paramagnetic resonance spectroscopy (agates)

with 5 mL concentrated HF and 3 mL concentrated HNO $_3$  at 50 °C (35 min). Rhenium solution (1 mL of 100  $\mu$ g/L concentration) was added as an internal standard and analysis was performed using a Perkin Elmer Sciex Elan 5000 quadrupole instrument with a cross-flow nebulizer and a rhyton spray chamber. The precision and accuracy of the ICP-MS measurements were evaluated by analysis of the glass sand reference material UNS-SpS (Monecke et al. 2000). The relative standard deviations for most analytes were below 10%.

Concentrations of Li, Be, Na, K, Rb, Ca, Sr, Mn, Sb, Zn, Fe, B, Al, Ga, Ge, Ti, P and U were analyzed on 200 µm polished thick sections of the samples by LA-ICP-MS on a double-focusing sector field mass spectrometer ELEMENT XR (Thermo-Instruments) coupled with a NewWave 193 nm excimer laser probe (Flem and Müller 2012). The laser had a pulse rate of 20 Hz, a scan-speed of 15 mm s<sup>-1</sup>, a spot size of 50 mm, and energy fluence of 5 to 7 mJ cm<sup>-2</sup> on the sample surface. The depth of ablation was ca. 50 µm. The carrier gas for transport of the ablated material to the ICP-MS was He-Ar mixture. External calibration was performed using three silicate glass reference materials (NIST SRM 610, 612, 614), the NIST SRM 1830 soda-lime float glass, the certified reference material BAM No.1 amorphous SiO<sub>2</sub> glass, and the Qz-Tu synthetic pure quartz monocrystal provided by Andreas Kronz from the Geowissenschaftliches Zentrum Göttingen (GZG), Germany. Each measurement comprised 15 scans of each isotope, with a measurement time varying from 0.15 s/scan for K in high resolution to 0.024 s/scan of, for example, Li in low resolution. A linear regression model, including several measurements of the different reference materials, was used to define the calibration curve for each element. For the calculation of P concentrations.

the procedure of Müller et al. (2008) was applied. Ten sequential measurements on the Qz-Tu synthetic pure quartz monocrystal were used to estimate the limits of detection (LOD, 3standard deviations of 10 measurements). The analytical error ranges within 10% of the absolute concentration of the element.

Fluid inclusions were examined in polished thick sections (100  $\mu$ m) of macrocrystalline quartz in the agate samples using a Linkam THMS 600 heating-freezing stage. Two synthetic fluid inclusion standards (SYN FLINC; pure H<sub>2</sub>O, mixed H<sub>2</sub>O–CO<sub>2</sub>) were used to calibrate the equipment. The precision of the system was  $\pm$  2 °C for homogenization temperatures (T<sub>h</sub>), and  $\pm$  0.2 °C in the temperature range between – 60 and + 10 °C.

#### Results

# Volcanic host rock and lithophysae

The macroscopic appearance of all investigated rocks and lithophsae samples from the distribution area of the Kemmlitz rhyolite is similar and is characterized by a porphyritic texture with yellowish-white aphanitic ground mass and numerous phenocrysts of quartz and feldspar (Fig. 2). Some of the feldspar phenocrysts are partially or completely altered and kaolinized. Pigmentation by iron compounds and/or bleaching can result in blotched colour variations. The cavities of the lithophysae are mostly filled with agate (chalcedony and macrocrystalline quartz), and sometimes clay minerals in interstices (Fig. 2c).



Table 2 Chemical composition of the massive porphyritic rhyolite (Zetzschlig) and lithophysae (other samples) (in wt%) analyzed by (XRF)

Oxide	Bör	Göt	Grö	Kem	Müg	Mut	Que	Rod	Wer	Zet
SiO <sub>2</sub>	77.85	81.08	72.19	81.46	76.09	80.97	80.74	79.84	82.31	79.79
$TiO_2$	0.08	0.07	0.27	0.11	0.09	0.12	0.08	0.09	0.09	0.07
$Al_2O_3$	12.31	10.46	14.89	5.92	12.63	9.84	10.13	10.30	9.32	11.45
$Fe_2O_3$	0.41	0.29	0.23	0.20	0.41	0.54	0.52	1.07	0.36	0.31
MgO	0.13	< 0.05	0.08	0.06	0.11	0.11	0.13	0.12	0.06	0.13
CaO	0.06	0.07	0.04	0.06	0.09	0.10	0.10	0.03	0.11	0.11
BaO	0.01	< 0.01	0.06	< 0.01	< 0.01	0.01	0.02	0.02	0.02	< 0.01
$Na_2O$	0.96	0.73	0.52	< 0.2	1.00	0.53	0.61	0.26	< 0.2	0.53
$K_2O$	6.79	5.84	9.82	< 0.1	7.77	5.95	5.68	6.96	6.58	6.38
$P_2O_5$	< 0.06	< 0.06	0.07	< 0.06	< 0.06	< 0.06	< 0.06	< 0.06	< 0.06	< 0.06
$ZrO_2$	0.01	0.01	0.02	0.02	0.02	0.03	0.02	0.02	0.02	0.01
LOI	1.6	1.4	1.7	12.4	1.3	1.4	1.6	1.5	1.1	1.4
Total	100.28	99.99	99.85	100.24	99.48	99.62	99.64	100.17	100.00	100.19

In all samples below the limit of detection:  $SO_3 < 0.3$ ,  $Mn_3O_4 < 0.03$ ,  $V_2O_5 < 0.01$ , SrO < 0.01, NiO < 0.01, PbO < 0.005, CuO < 0.01, ZnO < 0.005,  $Cr_2O_3 < 0.01$ ,  $HfO_2 < 0.01$ ;

Abbreviations of sample locations: Bör Börtewitz, Göt Göttwitz, Grö Gröppendorf, Kem Kemmlitz, Mut Mutzschen, Müg Mügeln, Que Querbitzsch, Rod Roda, Wer Wermsdorf, Zet Zetzschlig, LOI Loss of ignition

The chemical composition (Table 2) was used to evaluate the petrochemical classification of the investigated volcanic rocks. According to the classification diagram of Winchester and Floyd (1977) (Fig. 3) all rocks plot into the field of rhyolites (with exception of Gröppendorf that falls into rhyodacite/dacite field). Although Winchester and Floyd (1977) used immobile elements for their discrimination, a possible raise of the SiO<sub>2</sub> contents due to secondary silica supply during the alteration processes has to be taken into consideration.

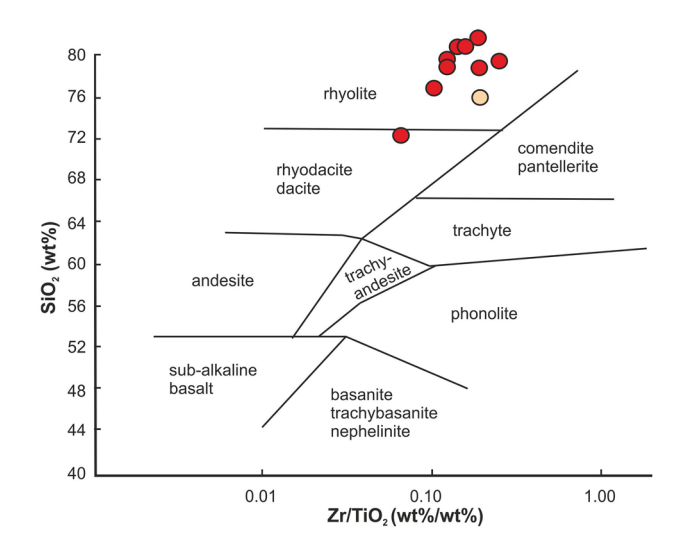


Fig. 3 Position of the investigated volcanic rocks in the classification diagram according to Winchester and Floyd (1977) (orange symbol=massive, porphyritic Kemmlitz rhyolite, red symbols=lithophysae)

Mineralogical characteristics (Table 3) are well-correlated with their whole rock geochemistry and also reflect the similarity of the rock samples of the Kemmlitz rhyolite. All samples have a monotonous mineral composition dominated by quartz and the two K-feldspar phases, i.e. sanidine and orthoclase as confirmed by XRD Rietveld refinement. It can be assumed that the high-temperature modification sanidine mainly represents the K-feldspar phenocrysts that crystallized early in the magma chamber, whereas most of orthoclase is a component of the fine-grained rock matrix. This is a common feature of these rocks and has been reported repeatedly (e.g. Repstock et al. 2018; Götze et al. 2020a).

**Table 3** Mineral composition (in wt%) of the volcanic rocks and lithophysae from the distribution area of the Kemmlitz rhyolite determined by XRD with Rietveld refinement

	Quartz	Sanidine	Orthoclase	Kaolinite
Börtewitz	48.2±0.6	$33.1 \pm 1.0$	$14.5 \pm 0.8$	$4.2 \pm 0.5$
Göttwitz	$55.6 \pm 0.6$	$30.5 \pm 1.2$	$10.8 \pm 1.0$	$3.1 \pm 0.5$
Gröppendorf	$28.0 \pm 0.5$	$51.0 \pm 1.3$	$16.4 \pm 1.1$	$4.6 \pm 0.5$
Kemmlitz	$86.1 \pm 0.5$	b.d.l.	b.d.l.	$13.9 \pm 0.5$
Mügeln	$40.0 \pm 0.5$	$43.1 \pm 1.1$	$14.2 \pm 1.0$	$2.7 \pm 0.4$
Mutzschen	$58.7 \pm 0.5$	$34.6 \pm 1.2$	$6.7 \pm 1.0$	b.d.l.
Querbitzsch	$58.5 \pm 0.7$	$25.6 \pm 1.2$	$13.7 \pm 1.0$	$2.2 \pm 0.4$
Roda	$53.2 \pm 0.5$	$43.8 \pm 1.2$	$3.0 \pm 1.1$	b.d.l
Wermsdorf	$58.1 \pm 0.6$	$36.9 \pm 1.1$	$5.0 \pm 0.8$	b.d.l
Zetzschlig	$48.9 \pm 0.6$	$40.1 \pm 0.9$	$5.2 \pm 0.7$	$5.8 \pm 0.5$

b.d.l. below detection limit

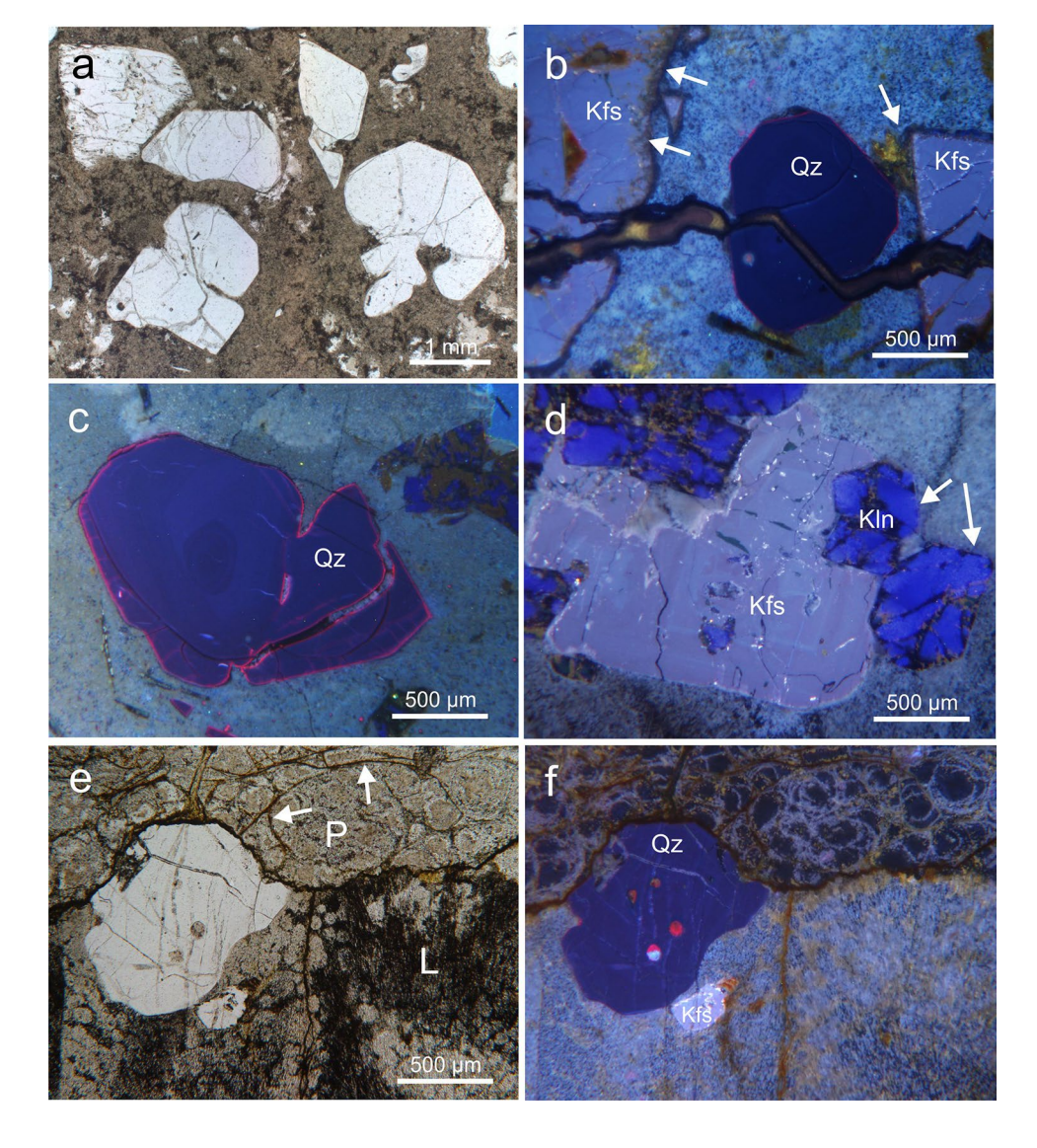


Plagioclase and minerals of the mica group were not detected in the samples, likewise as the accessory minerals such as apatite or zircon. All samples, excluding the lithophysae from Mutzschen, Roda and Wermsdorf contain variable amounts of kaolinite (up to 13.9 wt%), which was formed due to the alteration of pre-existing primary minerals (e.g. feldspar minerals). The mentioned three locations are situated outside the Kemmlitz kaolin district and therefore, were preserved from pervasive kaolinization. Elevated contents of kaolinite indicate the influence of weathering processes. The litophysa sample from Kemmlitz has the highest kaolinite content and no feldspar minerals were detectable.

Investigations by polarizing and CL microscopy confirm the similarities between massive volcanic host rocks and lithophysae. Both are characterized by a micro-crystalline matrix and large phenocrysts (Fig. 4a). Lithophysae frequently show areas with a spherulitic texture, which is often situated on marginal parts of the phenocrysts that probably acted as nucleus for crystallization. Sometimes the spherulitic texture is developed in large areas of the fine-grained rock matrix. Secondary fissures filled with silica penetrate the rock matrix and sometimes even cross-cut large phenocrysts (Fig. 4b). In general, the amount of phenocrysts varies between ca. 5 and 20% and likewise the size of the crystals. The average size of phenocrysts is ca. 1 mm.

Hypidiomorphic quartz crystals are the dominating phenocryst population with rounded edges and distinct features of resorption and corrosion. CL studies of the quartz crystals show very similar appearance in all samples. The quartz crystals exhibit deep blue luminescence with slight zoning and striking red rims (Fig. 4c). K-feldspar phenocrysts have bright blue luminescence and CL-contrasted growth zoning. The K-feldspar phenocrysts are relatively fresh and show only slight alteration features in marginal parts (brownish CL – Fig. 4b). The absence of plagioclase or biotite crystals in the rhyolites as already noted by XRD investigations

Fig. 4 a Plane-polarised transmitted-light image of massive, porphyritic Kemmlitz rhyolite (NW-Saxony, Germany) from the type locality "Am Zetzschlig"; the microtexture is characterized by fine-grained matrix with several hypidiomorphic quartz phenocrysts showing features of resorption and corrosion; b CL micrograph of a lithophysa from Börtewitz; both ground mass and phenocrysts (Qz = quartz, Kfs = K-feldspar) are cross-cut by a secondary silica fissure; the K-feldspar shows marginal alteration features (arrows); c large quartz phenocryst (Qz) in a lithophysa from Gröppendorf showing typical blue-violet colour with weak zoning and typical red rims under CL; d CL micrograph of a lithophysa from Querbitzsch with bright blue luminescing, zoned K-feldspar; the arrows point to almost completely kaolinized (Kln) former plagioclase crystals; e/f Micrographs in transmitted light and CL of the marginal part of a lithophysa (L) from Roda showing adhering residues of the surrounding pitchstone (P); the lithophysa has a spherulitic micro-texture, whereas the pitchstone shows typical perlitic cracks (arrows)





was confirmed by the microscopic studies. Based on the habit of completely kaolinized crystals it can be assumed that previously existing plagioclases were completely altered (Fig. 4d). In contrast, accessory apatite and zircon, which could not be found by XRD analyses, were sporadically detected due to their striking luminescence. Apatite mostly displays yellow CL due to Mn<sup>2+</sup> activation and zircon appears sporadically as euhedral crystals with yellow CL and distinct growth zoning.

A conspicuous feature of almost all investigated lithophysae is the detection of adherent residues of surrounding rock material. In contrast to the spherulitic texture of the lithophysae, the former enclosing wall rock has partially a glassy appearance with distinct perlitic cracks indicating signatures of volcanic glass (pitchstone – Fig. 4e/f). The CL properties of quartz and K-feldspar phenocrysts in the pitchstone are the same as observed in the lithophysae indicating the formation from the same melt.

# Alteration products of the volcanic host rocks

Field observations revealed that large areas of the Kemmlitz rhyolite underwent intensive surficial weathering. Several economic kaolin deposits in the Kemmlitz kaolin district are the result of these alteration processes (Gilg et al. 2003; Schwerdtner et al. 2007). Therefore, most lithophysae occur in a strongly altered rock matrix which does not really represent the composition of the primary volcanic host rocks (compare Fig. 2b). The lithophysae themselves are more resistant to weathering and alteration than the former surrounding volcanic rocks and can provide information about their mineralogy and geochemistry assuming that they derive from the same melt. In addition, the surrounding clay matrix of the lithophysae may also provide some indications concerning the initial composition of the former host rocks.

XRD measurements of such clay material embedding the lithophysae produced diffractograms with sharp peaks at 14.7°20 und 29.1°20 (d values of 7 and 3.5 Å; Co K $\alpha$ ) confirming the presence of kaolinite (Fig. 5a). These reflections disappear after heating up to 500–550 °C (Fig. 5b; Cu K $\alpha$  radiation) due to dehydroxylization (Brindley and Brown 1980). A broad peak around ~8°20 (12 Å) can be assigned to the 001-reflection of smectite-group minerals (Fig. 5a). The lack of a rational series of base reflections in the X-ray pattern indicates the existence of mixed-layer clays containing smectite layers.

This assumption is further confirmed by two diffuse reflections at  $\sim 16.2$  Å and  $\sim 30$  Å after treatment with ethylene glycol. The reflection at  $9.7^{\circ}2\theta$  (d=9.1 Å) probably results from the overlapping of the 001 and 003 base reflections of illite and smectite and indicates the existence of illite-smectite mixed-layer clay. The peak at 1.5 Å ( $73.2^{\circ}2\theta$ ; Fig. 5a) is characteristic for dioctahedral smectite layers.

According to the d-value of the ~9.1 Å reflection in the XRD pattern of the ethylene glycol treated sample (Fig. 5b), the amount of illite layers can be estimated at ca. 50–60% (Moore and Reynolds 1997). Therefore, the investigated material consists of partially ordered R1 illite(0.6)/smectite mixed-layer clay. The comparison of different grain-size fractions revealed that the fractions > 63  $\mu$ m and 2–63  $\mu$ m showed the dominance of quartz, sanidine and kaolinite, whereas the fraction < 2  $\mu$ m predominantly consists of R1 illite(0.6)-smectite mixed-layer minerals.

## Mineralogy and geochemistry of the agates

#### Mineralogy of secondary cavity fillings

The mineral composition of the cavities within the lithophysae strongly differs from that of the geode matrix as well as the volcanic host rocks. Most cavities are partly or completely filled with silica and the agates commonly display various colours and distinct banding (Fig. 2). In agates from the occurrences within kaolin deposits greyish and bluishwhite colours predominate (Fig. 2e). Quartz is not only developed as typical banded chalcedony or macrocrystalline quartz, but sometimes appears as euhedral crystals or forms pseudomorphs and perimorphs after preexisting minerals (probably carbonates, sulfates; Figs. 2c and 6a).

Lath-shaped pseudomorphs in the agates (Fig. 2c) could be found in different locations of the Kemmlitz rhyolite. Such lattice-bladed pseudomorphs have also been reported from other agate mineralization in Permian volcanics (Powolny et al. 2019). It is very hard to find relics of primary minerals in these pseudomorphs, since they completely consist of silica in most cases. Detailed investigations with microscopic and spectroscopic techniques revealed the existence of residual dolomite, barite and kaolinite in lath-shaped pseudomorphs (Götze et al. 2020a). It can be concluded that there was a primary hydrothermal mineralization of carbonates and sulfates, followed by secondary alteration/dissolution and replacement of primary minerals by silica. Free crystallized euhedral quartz crystals in the centre of the cavities also show features of hydrothermal formation (Fig. 6a).

In many agate-bearing lithophysae occurring in the area of kaolin deposits or in strongly kaolinized volcanic host rocks, the centre or interstices are filled with clay (Figs. 2c and 6b). XRD and SEM analyses revealed that the kaolinite occurring within the agates is of high crystallinity (Hinckley index of almost 1, similar to "geode kaolinite" from Keokuk/Iowa, USA; Hayes 1964) without any disorder or dickite. With that the kaolinite clearly differs from the bulk kaolinite of the surrounding kaolin deposits (Schwerdtner et al. 2007). It can be assumed that this kaolinite originates from secondary crystallization processes inside the geodes. The mineralizing fluids probably diffused into the cavities,



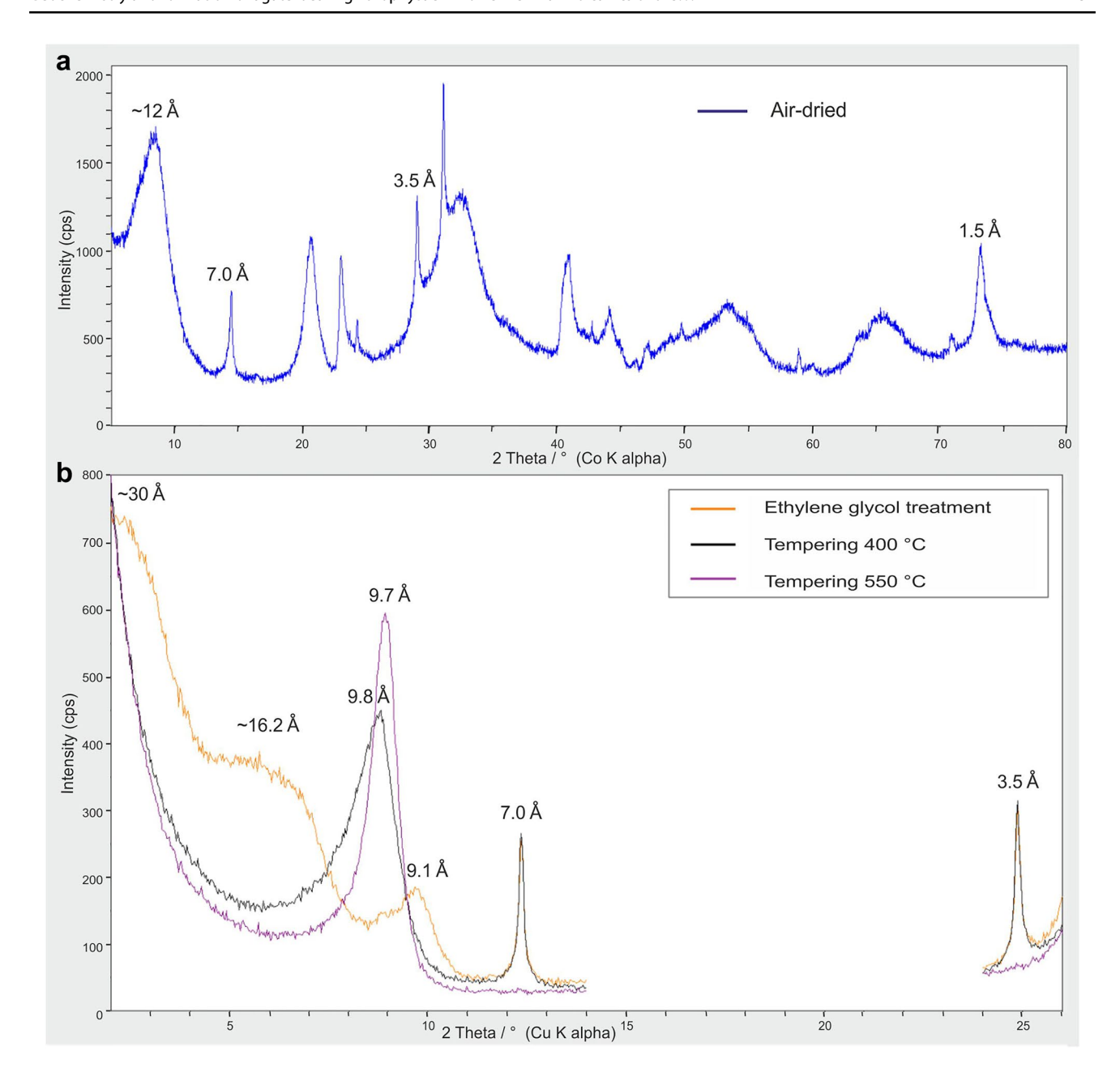


Fig. 5 X-ray diffraction patterns of the  $<2~\mu m$  fraction of the weathering crust surrounding an agate-bearing lithophysa from Mügeln (Saxony); a Overview (Co K alpha) of the whole analytical range (air dried); b Selected range (Cu K alpha) measured with oriented slide,

and saturated by ethylene glycol and tempered at 400  $^{\circ}$ C and 550  $^{\circ}$ C, respectively; the patterns in ethylene glycol saturated state and after tempering show the typical characteristics of illite-smectite mixed-layer clays

where a continuous crystallization under closed conditions was possible.

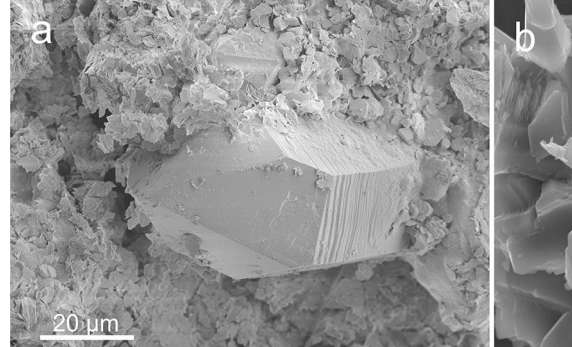
# Agate microstructure

The investigated agates in lithophysae from different locations within the Kemmlitz rhyolite show similar microtextures and CL properties (Fig. 7). The succession of silica minerals starts from the volcanic matrix and includes a

sequence of granular micro-crystalline quartz, fibrous bundle-like chalcedony and macrocrystalline quartz in the centre. Micrographs both in polarized light and CL indicate several generations of microcrystalline quartz.

Several generations start with spherulitic chalcedony on the top of the previous generation (Fig. 7a/b). The transition into macrocrystalline quartz is relatively smooth. The quartz crystals are homogeneous in polarized light, but show heterogeneous internal textures in CL (Fig. 7b). Distinct sector





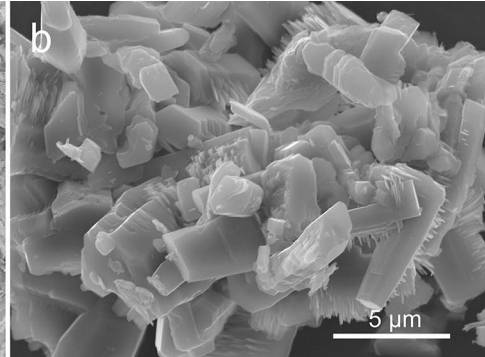


**Fig. 6** a SEM-SE image of the inner part of an agate geode from the kaolin deposit of Querbitzsch (Saxony) showing an euhedral quartz crystal overgrown by small crystal plates of kaolinite; the quartz crystal is characterized by horizontal stripes originating from intercalations of narrow rhombohedral and irregular vicinal planes dur-

ing probably hydrothermal growth of the prism planes; **b** perfectly crystallized kaolinite (according to XRD analyses - courtesy Reinhard Kleeberg) in the central part of an agate from Börtewitz with an uncommon euhedral, columnar habit and smooth crystal surfaces indicating its authigenic, non-replacive origin

zoning can probably be associated with growth under non-equilibrium conditions (Götze et al. 2020b).

The observed CL zoning in chalcedony correlates with the observed agate banding. Most agates are dominated by a bright yellow CL colour (Fig. 7c). Spectral measurements of this CL emission show a dominant broad emission band at ca. 570 nm and an additional one at  $\sim 650$  nm (Fig. 7d). The 570 nm emission is associated with high oxygen deficiency and local structural disorder in quartz (Götze et al. 2015). The CL spectra of the brownish-violet CL are dominated by the 650 nm emission band, which can be related to the non-bridging oxygen hole centre (NBOHC; Stevens-Kalceff 2009). Additional bands at 570 nm and 450 nm are developed as shoulders with varying intensities resulting in different shades of the visible brownish-violet luminescence colour (Fig. 7b, d). In several agate samples small radiation halos are visible (Fig. 7c), which point to micro-inclusions of radioactive material.

The identification and relative abundance of structural defects in the agates were determined by EPR measurements (Fig. 8). EPR spectroscopy at room temperature shows that the agates are different as compared with well-crystallized quartz as the following four centres have been recognized, i.e.  $E_1$ , #1, #3, and C (Fig. 8a; Mashkovtsev et al. 1978). The oxygen-vacancy electron centre  $E'_1$  is the most common defect centre in quartz resulting from various irradiations (Pan et al. 2008; Mashkovtsev et al. 1978). Centre #1 has been shown to be a superoxide radical associated with a silicon vacancy and a distant Al neighbour and the centre C is an ozonide radical also related to a silicon vacancy (Nilges et al. 2008; Pan et al. 2008). The unknown #3 centre (Mashkovtsev et al. 1978) is a certainly interesting defect, because its g-factor values and microwave power dependence are all intermediate between electron and hole centres.

Previous studies have shown that the centre #3 is prominent in quartz/agate with yellow CL (Götze et al. 2015).

The relative abundances of these four defect centres in the investigated agate samples vary widely. Most of the agates are dominated by the  $E_1$  electron centre and the unknown #3 centre, while #1 and C are almost invisible (Fig. 8b). The high abundances of these electron/hole centres also make accurate estimation of the Fe<sup>3+</sup> signals difficult (Sivaramiah et al. 2011). Moreover, the intensities of the silicon-vacancy hole centres are so high that they can overshadow a possible  $[AlO_4]^0$  centre at liquid-nitrogen temperature measurements.

#### Geochemistry and fluid inclusions of agates

Trace element data from separated macrocrystalline quartz and chalcedony as well as profiles across the agate banding are presented in Tables 4 and 5 as well as Fig. 9. The highest trace-element concentrations were measured for elements fixed with phases (e.g. alumosilicates) that occur in the surrounding rock matrix of the agates (i.e. Ca, Na, K, Al, Fe). In contrast, immobile elements such as Sc, Nb, Ta, Th or Ti show very low concentrations, sometimes below the detection limit of ICP-MS. The measured trace-element profile of the agate from Gröppendorf (Table 5) illustrates relatively balanced concentrations for most elements.

In general, trace element composition is far below the concentrations in the surrounding volcanic rocks, and the content in macrocrystalline quartz is lower than that in the associated chalcedony. However, there are specific chemical elements, which behave totally different. Remarkable high contents of B (29 ppm), Ge (> 18 ppm) and U (> 19 ppm) were detected in agates, which can exceed the average concentration of the Earth's crust (Clarke and Washington 1924) as well as the element concentration in the surrounding volcanic host rocks.



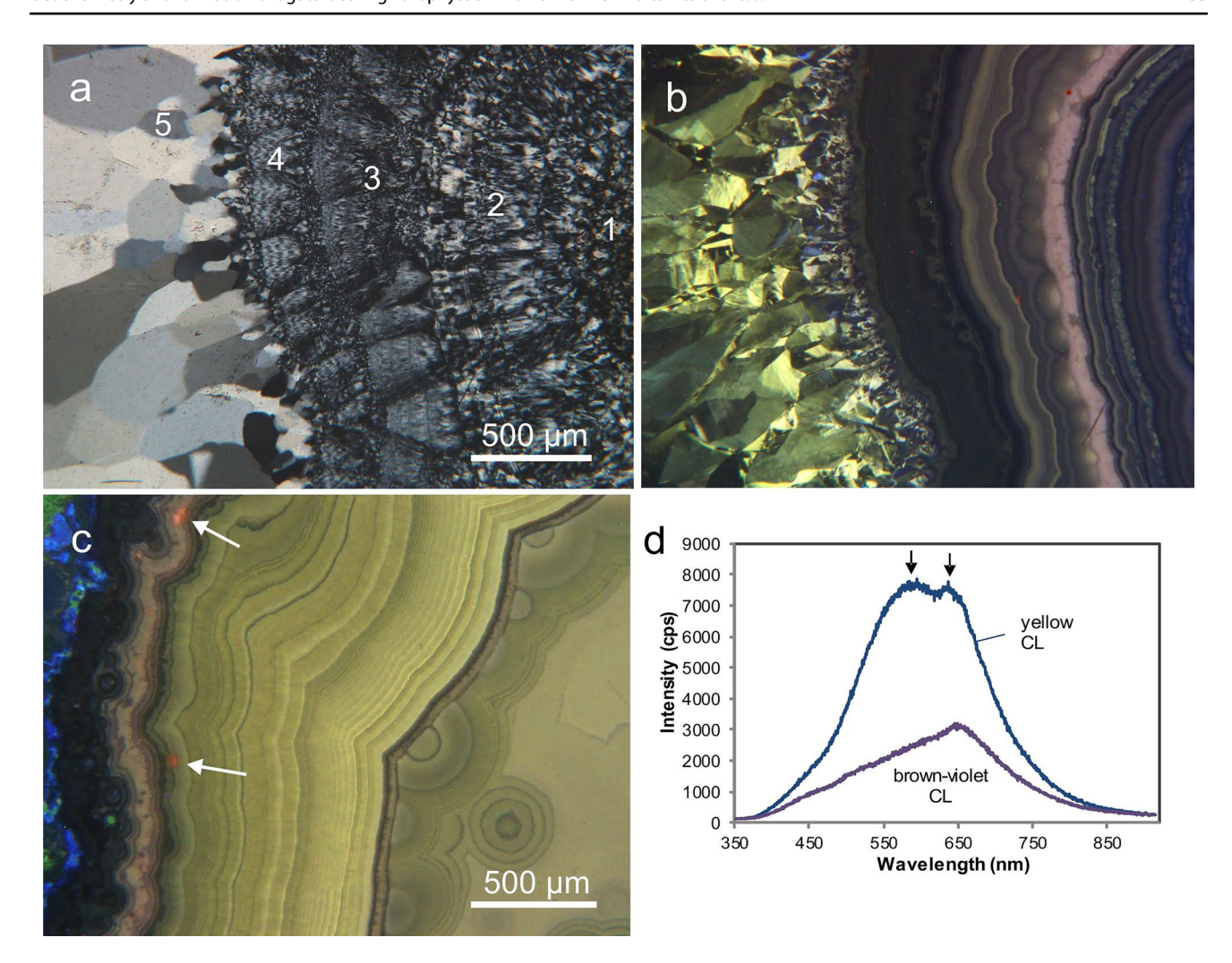


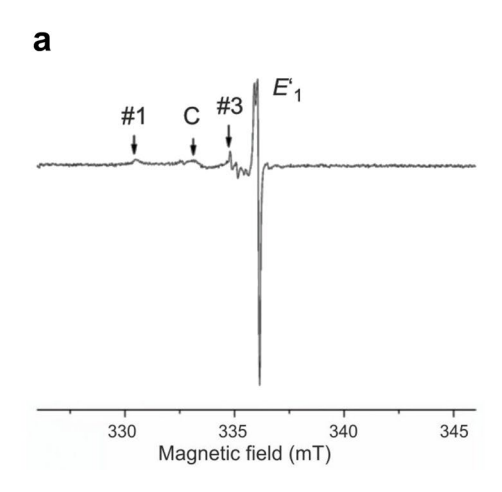
**Fig. 7** a/b Crossed-polarised transmitted-light (a) and CL (b) micrographs of an agate from Mutzschen (NW Saxony); the microstructure of silica mineralization develops from granular micro-crystalline quartz (1) via fibrous and/or bundle-like chalcedony (2–4) to macrocrystalline quartz in the centre (5); chalcedony shows brownish-violet CL whereas macrocrystalline (prismatic) quartz exhibits yellow CL with heterogeneous internal textures although appearing homogene-

ous in polarized light; **c** CL micrograph of an agate from Gröppendorf revealing mostly yellow luminescence; note the radiation halos (arrows) pointing to radioactive inclusions; **d** CL spectra of the two dominating luminescence types; yellow luminescent areas are dominated by a broad band at ~570 nm and a weak signal at 650 nm, whereas brown-violet CL exhibit an asymmetric signal comprising of a 650 nm emission band with a shoulder at lower wavelengths

The chondrite normalized REE distribution patterns for the agates exhibit pronounced negative Eu anomalies (Eu/Eu\*=0.004–0.16; [Eu/Eu\*=Eu<sub>n</sub>/(Sm<sub>n</sub> · Gd<sub>n</sub>)<sup>0.5</sup>]) and slight positive Ce-anomalies (1.23–1.55; Fig. 9). The normalized light rare earth elements (LREE) show an almost horizontal trend or have only a slight slope from La to Sm (La<sub>n</sub>/Sm<sub>n</sub> 0.64–2.38), whereas the pattern of the HREE from Gd to Yb is slightly increasing (Gd<sub>n</sub>/Yb<sub>n</sub> 0.31–1.13). The quartz sample reveals concave shape for HREE segments, whereas a convex shape is visible for HREE segments of chalcedony. Flat HREE segments are observed, in turn, for the volcanic host (lithophysae).

Fluid inclusion studies included measurements of homogenization temperatures and minimum formation temperatures as well as fluid salinities. In general, the inclusions in micro-crystalline chalcedony were too small to be measured though. Therefore, fluid inclusions were exclusively studied in macrocrystalline quartz of the agate centres. Although many fluid inclusions were detected, most of them are monophase inclusions of secondary origin (5–20  $\mu$ m in size) forming trails or arranged along fractures. In contrast, the number of measurable primary fluid inclusions in quartz was very low. The primary inclusions are heterogeneously distributed in the quartz crystals and have sizes between 10 and 30  $\mu$ m (Fig. 10). They occur as isolated inclusions or as inclusion clusters. If several fluid inclusions show similar behavior during heating/freezing and have the same degree of filling, they were merged as fluid inclusion assemblages (FIA). Results of FIA studies are presented in Table 6.





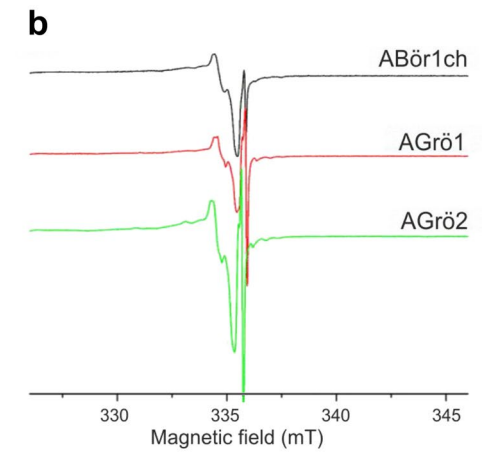


**Fig. 8** EPR spectra of investigated agate samples showing the electron/hole centres in the central magnetic field: **a** plot with the indicated four centres  $E_1$ , #1, #3 and C measured at a microwave power of 2 mW in a representative agate sample from Burgstall; **b** comparison of EPR spectra taken at a microwave power of 20 mW from

two agate samples from Gröppendorf (AGrö1=white chalcedony, AGrö2=dark chalcedony) with chalcedony of an agate sample from Börtewitz (ABör1ch) illustrating the dominance of the  $E^{\prime}_{1}$  electron centre and the #3 centre

Cryometric measurements show minimum formation temperatures for ice between -3 and -6 °C (average -4.72 °C), which can be assigned to salinities between 4.96 and 9.21 eq% NaCl (average 7.45 eq% NaCl). Measurements of the homogenization temperatures of the fluid inclusions provided temperatures between 134 and 186 °C. The locations slightly differ between each other but show relatively similar temperatures for one occurrence. However, the inclusions have different degrees of filling (i.e. liquid-vapour ratios with 10-30% gas bubbles) indicating the trapping of fluids under heterogeneous conditions. Accordingly, temperatures of homogenization cannot directly be used as trapping temperatures of the fluids. The lowest measured temperatures of homogenization then represent a minimum temperature of trapping. These minimum temperatures are 157 °C, 177 °C and 134 °C for Börtewitz, Mügeln and Gröppendorf, respectively.

Secondary fluid inclusions were not considered for the results of the present study. Their homogenization temperatures are significantly lower (70–80 °C), since they were formed along fractures and do not reflect the primary conditions of agate formation.

#### **Discussion**

# Formation of volcanic host-rocks and lithophysae

The chemical composition of the Kemmlitz rhyolite and associated lithophysae characterizes the rocks as rhyolites (Fig. 3). The mineralogical investigations revealed a

common monotonic mineral assemblage that is dominated by quartz and the two K-feldspar phases sanidine and orthoclase (compare Table 3). The high contents of sanidine point to high formation temperatures and rapid cooling of the acidic melt. Quartz phenocrysts exhibit a deep blue CL and weak zoning. The marginal parts of the grains are characterized by red luminescent rims, which are probably caused by reactions with the surrounding melt. The observed growth embayments are generally interpreted to be caused by foreign particles, which adhere at the growing surface, hindered further growth at that place and resulted in lobate embayments (e.g. Müller et al. 2010). The red CL rims and the frequent development of embayments most likely result from a rapid disequilibrium crystallization of quartz phenocrysts in the magma chamber (Barbee et al. 2020).

In contrast to literature data (e.g., Röllig 1976; Eigenfeld 1978), plagioclase, biotite and pyroxene were not found in the investigated rhyolites and lithophysae. However, the morphology of completely kaolinized lath-shaped phenocrysts indicates the existence of primary plagioclase crystals that were completely altered to clay minerals. These secondary alteration processes are responsible for slight variations in the chemical composition of the otherwise homogeneous rocks.

The presence of hypidiomorphic quartz and well preserved K-feldspar phenocrysts, and the lack of glass shards and fiamme indicate that the volcanic rocks derive from lava flows and are not related to ignimbrites. Based on field observations, Eigenfeld (1978) related the lavas forming the Kemmlitz rhyolite to the existence of a stratovolcano and supposed the volcanic extrusion centre close to the recent kaolin deposit of Kemmlitz.



**Table 4** Trace-element concentrations (in ppm) analyzed by solution ICP-MS, and element ratios of agate samples from Mügeln (AMüg), Börtewitz (ABör) and Gröppendorf (AGrö)

	AMüg-R	AMüg-Q	AMüg-Ch	ABör-Ch	AGrö-Ch
Al	n.a.	56.7	1160	1510	168
Ba	174	< 1.0	38.0	64.8	5.34
Ca	902	< 1.00	226	190	< 100
Co	1.90	0.063	0.17	0.19	0.02
Cr	1.89	1.02	1.20	0.81	0.64
Cs	5.59	0.039	0.84	1.69	0.19
Cu	5.64	0.73	0.82	2.62	0.76
Fe	n.a	4.63	10.1	2.57	1.67
Ge	1.58	4.37	4.86	2.11	16.6
K	n.a	< 50	169	411	60.1
Li	42.9	0.51	2.27	12.6	0.49
Mg	259	4.60	28.5	49.0	10.9
Mn	13.8	0.90	2.65	3.71	0.81
Na	9550	34.7	168	234	58.2
Nb	25.1	0.49	0.53	0.92	0.56
Rb	264	0.41	2.26	4.53	0.48
Sb	7.91	0.10	72.5	13.7	4.83
Sc	1.83	0.21	0.57	0.25	0.18
Sr	17.1	0.11	3.68	7.77	0.62
Ta	1.65	< 0.1	< 0.1	< 0.1	< 0.1
Th	20.4	< 0.5	0.72	0.62	< 0.5
U	6.53	0.19	19.4	13.7	1.08
Zn	10.9	10.1	4.63	2.57	1.67
Y	34.6	0.022	3.37	9.77	2.66
La	16.9	0.037	0.369	0.407	0.032
Ce	44.3	0.130	1.14	1.19	0.095
Pr	4.39	0.011	0.104	0.132	0.008
Nd	16.0	0.043	0.420	0.552	0.038
Sm	3.65	0.009	0.157	0.263	0.029
Eu	0.223	0.0002	0.001	0.0005	0.0005
Gd	4.49	0.006	0.338	0.686	0.102
Tb	0.943	0.001	0.083	0.195	0.033
Dy	5.93	0.005	0.591	1.62	0.298
Но	1.25	0.001	0.126	0.39	0.074
Er	3.67	0.003	0.357	1.26	0.277
Tm	0.543	0.0005	0.051	0.182	0.046
Yb	3.38	0.004	0.311	1.07	0.245
Lu	0.487	0.001	0.044	0.145	0.029
La <sub>n</sub> /Yb <sub>n</sub>	2.78	5.14	0.66	0.21	0.07
La <sub>n</sub> /Sm <sub>n</sub>	2.68	2.38	1.36	0.89	0.64
Gd <sub>n</sub> /Yb <sub>n</sub>	0.99	1.13	0.82	0.48	0.31
Eu/Eu*	0.16	0.06	0.01	0.004	0.03
Ce/Ce*	1.24	1.55	1.40	1.23	1.43

Normalization is based on data given by Anders and Grevesse (1989) Eu anomaly  $Eu/Eu^* = Eu_n/(Sm_n \cdot Gd_n)^{0.5}$ ; Ce anomaly  $Ce/Ce^* = Ce_n/(La_n \cdot Pr_n)^{0.5}$ 

Q macrocrystalline quartz, Ch chalcedony, R surrounding volcanic host rock, i.e. lithophysa, n.a. not analyzed

**Table 5** Results (in ppm) of spatially resolved trace-element analysis by LA-ICP-MS of an agate from Gröppendorf

•		Č	11		
	LOD	AGrö-1 Margin	AGrö-2	AGrö-3	AGrö-4 Core
Li	0.13	0.71	0.91	0.71	0.58
Be	0.01	0.52	0.69	0.45	0.49
В	0.68	29.0	15.4	15.2	21.3
Mn	0.08	0.78	0.98	0.60	0.65
Ge	0.05	14.7	18.6	12.8	13.0
Rb	0.03	0.56	0.51	0.44	0.46
Sr	0.01	0.55	0.58	0.61	0.49
Sb	0.02	4.55	5.53	4.53	3.72
U	0.10	1.06	1.14	1.00	1.02
Na	10.5	48.2	58.6	40.1	48.6
Al	4.55	203	185	170	189
P	0.98	1.87	0.30	2.47	2.38
K	18.7	66.4	63.5	47.3	61.7
Ca	6.01	79.2	83.5	76.4	104
Fe	0.80	12.4	14.6	0.84	13.2
Zn	1.48	-	0.56	2.43	1.08
Ga	0.01	2.06	1.38	1.49	1.08

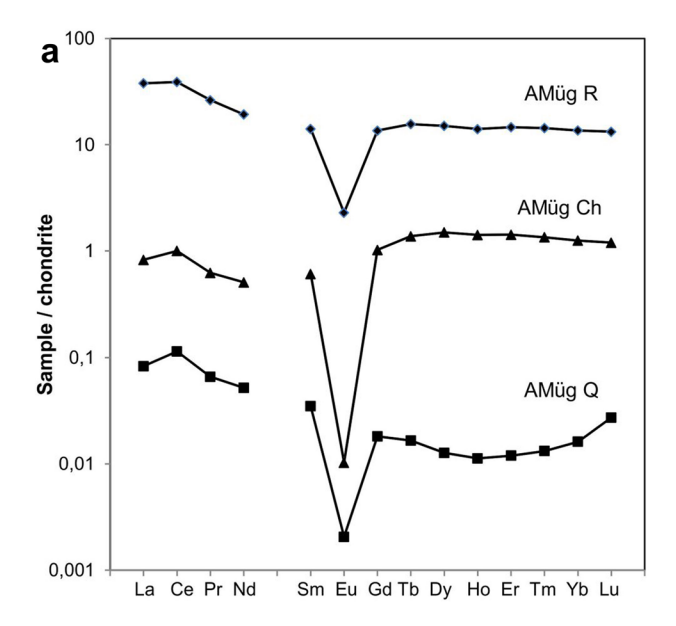
Analysis points are shown in Fig. 2E. Ti was below 1.28 ppm in all samples

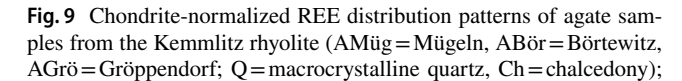
LOD limit of detection

The detected similarities in the mineral and chemical composition of the volcanic host rocks and associated lithophysae indicate a formation during the same volcanic event that formed the Kemmlitz rhyolite. The consistent appearance of phenocrysts and their CL properties in lithophysae and the massive lithophysae-free rhyolite can be explained by their formation from the same melt reservoir. Lithophysae developed during magma cooling in marginal parts and fluid-rich zones of the volcanic body. They represent hightemperature crystallization domains in silica-rich volcanic rocks comprising one or more cavities. They especially form during cooling of high-silica melts with an enhanced volatile content (Agangi et al. 2010), and it is assumed that lithophysal cavities develop above the melt/glass transformation temperature Tg due to several factors including tensional stress (Breitkreuz 2013).

Despite the similarities in geochemistry, mineralogy and phenocryst characteristics of the common porphyritic Kemmlitz rhyolite and lithophysae, no high temperature crystallization domains could be found in the massive, porphyric volcanic host rock. Instead, marginal relics of pitchstone on the lithophysae indicate their exclusive formation in a glassy facies (pitchstone). This conclusion is emphasized by the frequent occurrence of agate-bearing lithophysae in a matrix of illite-smectite (I-S) mixed-layer minerals, which

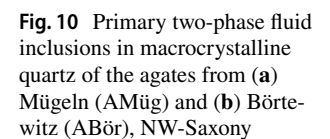


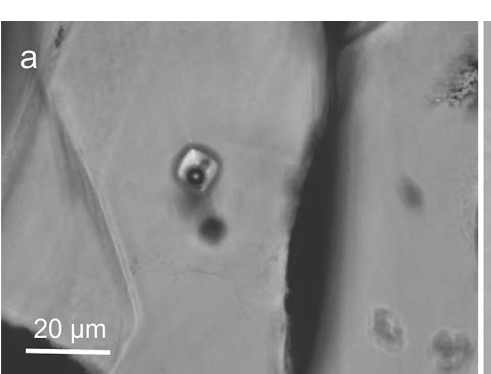


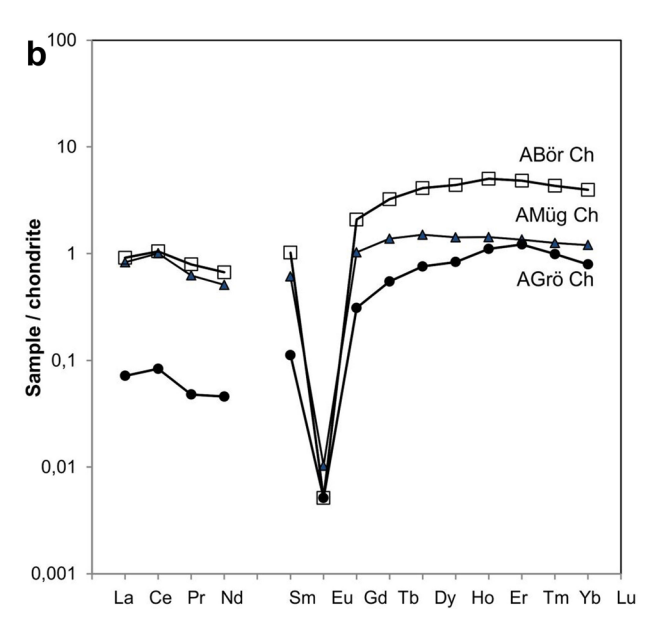


result from the alteration of the former surrounding glassrich volcanic host rocks. Even in kaolin deposits, field observations proved the occurrence of lithophysae in restricted areas with elevated contents of illite-montmorillonite mixed layer clays (Schwerdtner et al. 2007).

Investigations of Gilg et al. (2003) evidenced that the economic kaolinization of the porphyritic rhyolite occurred during Tertiary, whereas I-S mixed-layer minerals formed exclusively at the expense of silicic volcanic glass and not from feldspar. They assume that the I-S may have formed as a result of low-temperature illitization of smectite by K-rich solutions from initially glass-rich protoliths during long reaction times (~100 Ma during Jurassic to Triassic). Our field observations confirmed that agate-bearing lithophysae occur exclusively in areas with high I-S contents (up to 30 wt%) besides kaolinite and quartz in the surrounding weathered material. This is another strong indication that the lithophysae formed preferentially in a glassy matrix







AMügR represents the data of the surrounding volcanic rock (lithophysa); normalization according to data of Anders and Grevesse (1989)

(pitchstone). It is not clear yet, whether these pitchstones represent a glassy facies in marginal parts of the volcanic massif or a vein-like pitchstone formation as it was found in other parts of the NW-Saxonian Volcanic Complex (Götze et al. 2020a).

#### Origin and geochemistry of agates

# Geochemistry of agates and origin of silica

Assuming that trace elements in agate were incorporated during the process of agate formation, they represent important geochemical indicators for the origin of the mineral-forming fluids and the specific conditions of crystallization. The trace-element data of the different occurrences (Tables 4 and 5) reveal similar concentration levels of most chemical elements in the investigated agates pointing to comparable conditions of formation.

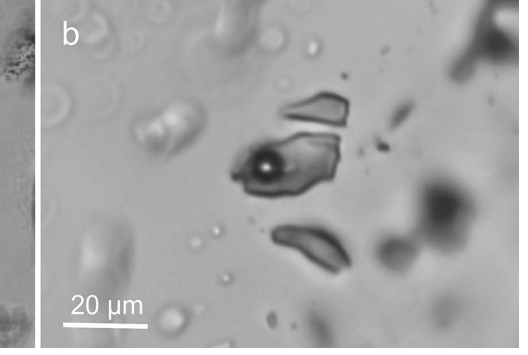




**Table 6** Measured fluid inclusion data of quartz in agates from Mügeln (AMüg), Gröppendorf (AGrö) and Börtewitz (ABör)

Sample/inclusion	T <sub>h</sub> (°C)	Density (g/cm <sup>3</sup> )	T <sub>m</sub> ice (°C)	Salinity (eq.% NaCl)	T <sub>m</sub> salt (°C)	salinity (eq% NaCl)
AMüg-1 SI	177	0.932	-3.3	5.41	-12.6	24.42
AMüg-2 SI	184	0.929	-3.7	6.01	-12.2	24.48
AMüg-2 SI	186	0.919	-3.0	4.96	-12.8	24.39
AMüg-3 SI	181	0.931	-3.6	5.86	-12.0	24.51
AGrö-1 FIA	134	0.984	-4.6	7.31	-13.2	24.33
AGrö-3 SI	137	0.980	-4.5	7.17	-13.4	24.30
AGrö-4 FIA	139	0.982	-4.9	7.73	-13.5	24.29
ABör-1 SI	157	0.960	-4.2	6.74	-13.0	24.36
ABör-2 SI	158	0.958	-4.0	6.45	-12.8	24.39
ABör-4 FIA	158	0.964	-4.6	7.31	-13.3	24.32

Calculation of density according to Brown and Lamb (1989)

Th homogenization temperature, FPD freezing point depression,  $T_m$  melting temperature, SI single inclusion, FIA fluid inclusion assemblage

It is obvious, that in particular chemical elements from the volcanic rock matrix (Al, Fe, Ca, Na, K) occur at elevated concentrations in the SiO<sub>2</sub> matrix of the agates. The concentrations are often higher in chalcedony compared to the associated macrocrystalline quartz of the agate centres. There are strong indications that these elements are released and mobilized together with SiO<sub>2</sub> from the surrounding rocks during late or post-volcanic alteration. Other indications for such processes are given by the very low concentrations of immobile elements such as Sc, Nb, Ta, Th and Ti that are sometimes below the detection limit of ICP-MS (Table 4).

A conspicuous feature of the investigated agates is the enrichment of B, Ge and U (Table 5) according to the point measurements by ICP-MS. The measured concentrations are far higher than in quartz of magmatic or metamorphic rocks (Blankenburg et al. 1994). Previous investigations have shown that chemical transport reactions (CTR) of gases and liquids can probably explain the transport of specific chemical elements better than their exclusive transport by aqueous solution (Götze et al. 2012). Therefore, the elevated concentrations of B, Ge, and U in quartz could be explained with common CTR of Si, B, Ge or U by stable fluorine compounds such as SiF<sub>4</sub>, BF<sub>3</sub>, GeF<sub>4</sub> or UO<sub>2</sub>F<sub>2</sub>. In consequence, it can be assumed that other fluids than pure H<sub>2</sub>O participate in the alteration and transport processes. Whereas Ge and B can be incorporated into the quartz structure, recent studies have shown that U can be trapped as the uranyl ion in a stable uranyl-silicate complex (Pan et al. 2021).

Further indications concerning the proposed alteration and fractionation processes are given by the observed REE distribution patterns in the agates (Fig. 9). The pronounced negative Eu-anomalies, the detected Ce-anomalies, as well as the enrichment of heavy REE could be explained by the interaction of the volcanic host rocks with magmatic

volatiles and heated meteoric water resulting in the preferred complexation of released HREE by carbonate- and/ or F-complexes during the alteration and transport processes (Wood 1990). Indications for the mixing of extremely different compounds (e.g. volatiles, meteoric water) are provided by the presence of Ce anomalies in the agates (Kempe et al. 1997).

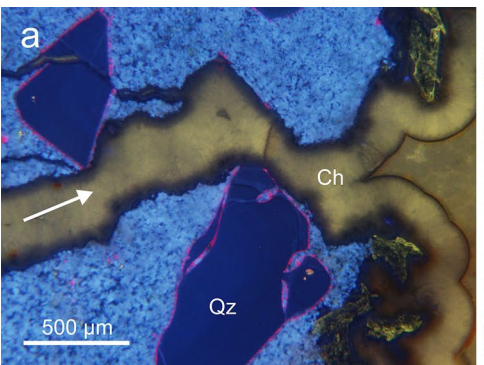
#### SiO<sub>2</sub> microstructure and mechanism of agate formation

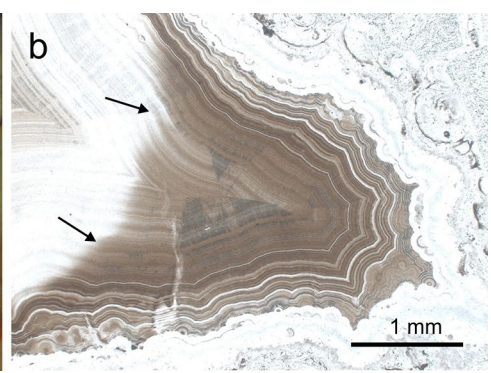
Observations in numerous agate-bearing lithophysae revealed that the process of geode filling and agate formation was probably a multi-step type. Agates do not only occur as banded chalcedony and macrocrystalline quartz, but SiO<sub>2</sub> mineralization also includes pseudomorphs and perimorphs after preexisting minerals (probably carbonates, sulfates) or small crystals of euhedral quartz (Figs. 2 and 6). These features can be explained by a primary hydrothermal mineralization followed by secondary alteration/dissolution and replacement of primary minerals by silica. The observed "Bambauer lamellae" on the euhedral quartz crystals (Fig. 6a) also show features of hydrothermal formation (Rykart 1995).

Temperatures of agate formation were calculated from the results of fluid inclusion studies, which yielded minimum homogenization temperatures of 134 °C for agates from Gröppendorf, 157 °C for Börtewitz and 177 °C for Mügeln (Table 6). Although the measurements were only possible in macrocrystalline quartz of the agates, the results indicate relatively high formation temperatures. Therefore, it can be assumed that the mobilization and accumulation of silica started already during a late phase of or soon after the volcanic activity. Microscopic and CL studies emphasized that the supply of silica must have occurred after the crystallization and solidification of the lithophysae, since the silica



Fig. 11 a CL micrograph of an agate-bearing lithophysae from Börtewitz showing the supply of secondary silica (yellow CL) via small cracks and fissures (arrow; Qz = quartz phenocryst, Ch = secondary chalcedony); b Plane-polarised transmittedlight image of an agate from the kaolin deposit Gröppendorf showing features of surficial bleaching processes (arrows)





was supplied via small fissures along fractures through the rock matrix of the lithophysae or even large phenocrysts of quartz or K-feldspar (Fig. 11a).

The crystallization of the silica matrix in the agates mostly started with the formation of spherulites and continues inwards to the agate centre with fibrous chalcedony and macrocrystalline quartz. Spherulitic growth is a characteristic feature of crystallization processes from amorphous (noncrystalline) precursors (Gránásy et al. 2005). CL microscopy revealed the development of several successive crystallization fronts, each starting on the top of the former one indicating discontinuous silica supply. The formation and development of the typical agate micro-structure can be explained by the crystallization and stepwise self-organization of SiO<sub>2</sub> (e.g., Wang and Merino 1990; Heaney 1993; Ortoleva et al. 1994). The ongoing silica release due to the crystallization of chalcedony results in a residual aqueous medium with low silica concentration. Accordingly, the crystallization front becomes morphologically stable and macrocrystalline quartz with lower amounts of impurity elements forms in the agate centre.

The results of CL microscopy and spectroscopy revealed the dominance of yellow luminescent chalcedony and macrocrystalline quartz. This broad band CL emission at ~ 570 nm can be attributed to high oxygen deficiency and local structural disorder in quartz (Götze et al. 2015). Oxygen deficiency is confirmed by the results of EPR measurements showing the dominance of  $E'_1$  centres, which are related to oxygen vacancies. The close relationship between the yellow CL emission and high concentrations of defect centres as well as the specific geological environments were interpreted to be related to low temperature (mostly < 250 °C) processes of fast crystallization, probably from a non-crystalline precursor (Götze et al. 2015). Moreover, the irregular internal textures and sector zoning in macrocrystalline quartz point to crystallization under nonequilibrium conditions.

Chalcedony sometimes displays a violet brownish CL (650 nm emission band), which can be related to the non-bridging oxygen hole centre (NBOHC; Siegel and Marrone

1981). A number of different precursors of this NBOHC have been proposed, such as silanol groups, Na-impurities, or strained Si–O bonds (Stevens-Kalceff 2009). High values of silanol groups in chalcedony originating from an aqueous crystallization medium can be assumed, which are probably responsible for this specific CL behaviour (Flörke et al. 1982; Götze et al. 1999).

In some of the agates kaolinite was detected as last mineralization sequence filling interstices between chalcedony and/or residual voids within the agate geodes (Fig. 2c). Kaolinite in the agate nodules was exclusively found in agatebearing lithophysae within the kaolin deposits. It can be assumed that this mineralization was caused by the secondary influx of alteration fluids from the intensive surface kaolinization processes long after the formation of the agates. Since crystallization inside the geodes occurred in closed and undisturbed system, the formation of high-crystallinity kaolinite has been enhanced. Indications of such secondary processes can also be found in secondary bleaching effects of the agates in the kaolin deposits (Fig. 11b). The interaction of surficial weathering, kaolinization and the influence of surficial humic acids may have resulted in the alteration of the primary agate colours.

#### **Conclusions**

The present paper presents results of geochemical and mineralogical investigations of the Lower Permian Kemmlitz rhyolite within the NW-Saxonian Basin (Germany) and associated agate-bearing lithophysae (high-temperature crystallization domains). The results provide new data concerning the genesis and characteristics of these volcanic rocks and the origin of the lithophysae-hosted agate mineralization.

Based on their chemical composition (i.e. high  ${\rm SiO_2}$  contents) the volcanic rocks can be classified as rhyolites, whilst their phase composition is dominated by quartz, sanidine and orthoclase. The predominance of hypidiomorphic quartz phenocrysts, well preserved K-feldspar as well as the lack of glass shards and fiamme indicate that the volcanic rocks



derive from lava flows and are not related to ignimbrites. The consistent appearance of the phenocrysts and their cathodoluminescence (CL) characteristics indicate an origin from a common melt source. Detected variations in mineral composition are mainly related to secondary alteration processes, which partly resulted in the formation of economic kaolin deposits.

Agate-bearing lithophysae occur exclusively in distinct areas of the Kemmlitz rhyolite and have not been found within the massive porphyritic core facies. Instead, marginal relics of pitchstone on some of the lithophysae indicate their formation in a glassy facies (pitchstone). This conclusion is emphasized by the frequent occurrence of agate-bearing lithophysae in a matrix of illite-smectite mixed-layer clays, which result from the complete alteration of the former glass-rich volcanic host rocks.

The results of the study show that agate formation can be related to the alteration of the volcanic rocks accompanied by the infill of mobilized silica into cavities of lithophysae. Based on homogenization temperatures of fluid inclusions in macrocrystalline quartz of the agates it can be assumed that temperatures of these processes might have exceeded 150 °C. These elevated temperatures indicate a mobilization and accumulation of silica already during a late phase of or soon after the volcanic activities. Such a scenario is confirmed by the chemical composition of the agates, which is characterized by elevated concentrations of chemical elements of the volcanic rock matrix (Al, Ca, Fe, Na, K) that were released during the host rock alteration and were further accumulated in the silica matrix of the agates. In addition, remarkably high concentrations of B, Ge and U were measured in the agates, which exceed the element concentrations in the surrounding host rocks. Chondrite-normalized REE distribution patterns with enriched HREE, pronounced negative Eu-anomalies and slightly positive Ce-anomalies may be the result of interactions of magmatic volatiles (F/ Cl, CO<sub>2</sub>) and heated meteoric water with the volcanic host rocks.

The process of agate formation probably started with the accumulation and condensation of silicic acid and the formation of amorphous silica as precursors for the development of the typical agate structures. The typical crystallization succession includes spherulitic growth of chalcedony continuing into chalcedony "fibres" and finally macrocrystalline quartz when the SiO<sub>2</sub> concentration in the mineralizing fluid is low. Characteristic yellow CL, heterogeneous internal textures as well as high defect densities in the silica matrix of the agates all emphasize such a crystallization processes via an amorphous silica precursor under non-equilibrium conditions.

**Supplementary Information** The online version contains supplementary material available at https://doi.org/10.1007/s00710-023-00841-2.

Acknowledgements We thank Ulrich Georgi (Belgern, Germany) and Christoph Breitkreuz (Freiberg, Germany) for the kind allocation of sample material and the help during field work. Reinhard Kleeberg, Michael Magnus, Franziska Lessig, Fabian Gotsch, Matthias Burisch, Diana Ebert and Alexander Plessow (Freiberg, Germany) are gratefully acknowledged for their help during the analytical work and with sample preparation, respectively. Reviews of Tomasz Powolny and an anonymous expert improved the quality of the manuscript significantly. We also thank Nikita Chukanov and the editor-in chief Lutz Nasdala for helpful comments and their thorough editorial handling.

Funding Open Access funding enabled and organized by Projekt DEAL.

**Open Access** This article is licensed under a Creative Commons Attribution 4.0 International License, which permits use, sharing, adaptation, distribution and reproduction in any medium or format, as long as you give appropriate credit to the original author(s) and the source, provide a link to the Creative Commons licence, and indicate if changes were made. The images or other third party material in this article are included in the article's Creative Commons licence, unless indicated otherwise in a credit line to the material. If material is not included in the article's Creative Commons licence and your intended use is not permitted by statutory regulation or exceeds the permitted use, you will need to obtain permission directly from the copyright holder. To view a copy of this licence, visit http://creativecommons.org/licenses/by/4.0/.

#### References

Agangi A, Kamenetsky VS, McPhie J (2010) The role of fluorine in the concentration and transport of lithophile trace elements in felsic magmas: insights from the Gawler Range Volcanics, South Australia. Chem Geol 273:314–325

Anders E, Grevesse N (1989) Abundances of the elements: Meteoritic and solar. Geochim Cosmochim Acta 53:197–214

Barbee O, Chesner C, Deering C (2020) Quartz crystals in Toba rhyolites show textures symptomatic of rapid crystallization. Am Mineral 105:194–226

Blankenburg HJ, Götze J, Schulz H (1994) Quarzrohstoffe. Deutscher Verlag für Grundstoffindustrie, Leipzig-Stuttgart, p 296

Breitkreuz C (2013) Spherulites and lithophysae – 200 years of investigation on high-temperature crystallization domains in silica-rich volcanic rocks. Bull Volcanol 75:705–720

Breitkreuz C (2016) Die Vulkanite und Subvulkanite im Geopark Porphyrland: Ein spätpaläozoischer Supervulkankomplex. Schriftenreihe Dt Ges Geowiss 88:67–72

Brindley GW, Brown G (1980) Crystal structures of clay minerals and their X-ray identification. Mineral Soc Monogr No. 5, London, 494 pp

Brown PE, Lamb WM (1989) P-V-T properties of fluids in the system H<sub>2</sub>O-CO<sub>2</sub>-NaCl: new graphical presentations and implications for fluid inclusion studies. Geochim Cosmochim Acta 53:1209-1221

Clarke FW, Washington HS (1924) The Composition of the Earth's Crust. US Geol Survey Prof Paper, Reston, Virginia, USA, 117 pp

Doebelin N, Kleeberg R (2015) Profex: a graphical user interface for the Rietveld refinement program BGMN. J Appl Crystall 48:1573–1580

Eigenfeld F (1978) Zur geologischen Entwicklung der vulkanischen Gesteine im Süd- und Ostteil des NW-Sächsischen Vulkanitkomplexes. PhD thesis, Martin-Luther University Halle-Wittenberg, 236 pp

Flem B, Müller A (2012) In situ analysis of trace elements in quartz using Laser ablation inductively coupled plasma mass spectrometry. In: Götze J, Möckel R (eds) Quartz: Deposits, Mineralogy and Analytics. Springer, Berlin/Heidelberg, Germany, pp 219–236

Flörke OW, Köhler-Herbertz B, Langer K, Tönges I (1982) Water in microcrystalline quartz of volcanic origin: agates. Contrib Mineral Petrol 80:324–333



- Gilg HA, Weber B, Kasbohm J, Frei R (2003) Isotope geochemistry and origin of illite-smectite and kaolinite from the Seilitz and Kemmlitz kaolin deposits, Saxony, Germany. Clay Miner 38:95–112
- Glässer W (1983) Beitrag zur Petrologie und Vulkanologie der andesitoiden Vulkanite Nordwestsachsens. Hallesches Jb Geowiss 8:1–30
- Gold C (2011) Sedimentologie und Paläontologie frühpermischer Seen des Nordwestsächsischen Vulkanitkomplexes und des Thüringer-Wald-Beckens – Fallstudien zur Paläolimnologie. Master thesis, TU Bergakademie Freiberg, Germany, 86 pp
- Götze J, Plötze M, Fuchs H, Habermann D (1999) Defect structure and luminescence behaviour of agate results of electron paramagnetic resonance (EPR) and cathodoluminescence (CL) studies. Mineral Mag 63:149–163
- Götze J, Schrön W, Möckel R, Heide K (2012) The role of fluids in the formation of agate. Geochemistry 72:283–286
- Götze J, Pan Y, Stevens-Kalceff M, Kempe U, Müller A (2015) Origin and significance of the yellow cathodoluminescence (CL) of quartz. Am Mineral 100:1469–1482
- Götze J, Lessig F, Möckel R, Georgi U (2017) Zur Mineralogie von Vulkaniten im Bereich des Kemmlitzer Porphyrs. Veröff Museum Naturkunde Chemnitz 40:133–150
- Götze J, Möckel R, Breitkreuz C, Georgi U, Klein A (2020a) Zur Mineralogie von Vulkaniten und Lithophysen im Bereich des unterpermischen Leisniger Porphyrs (Nordwestsächsisches Becken). Veröff Museum Naturkunde Chemnitz 43:5–44
- Götze J, Möckel R, Pan Y (2020b) Mineralogy, geochemistry and genesis of agates a review. Minerals 10:1037
- Gránásy L, Pusztai T, Tegze G, Warren JA, Douglas JF (2005) Growth and form of spherulites. Phys Rev E 72:011605–011619
- Hayes JB (1964) Geodes and concretions from the Mississippian Warsaw Formation. Keokuk region, Iowa, Illinois. Missouri J Sed Petrol 34:123–133
- Heaney PJ (1993) A proposed mechanism or the growth of chalcedony. Contrib Mineral Petrol 115:66–74
- Hoffmann U, Breitkreuz C, Breiter K, Sergeev S, Stanek K, Tichomirova M (2013) Carboniferous-Permian volcanic evolution in Central Europe U/Pb ages of volcanic rocks in Saxony (Germany) and northern Bohemia (Czech Republic). Int J Earth Sci 102:73–99
- Hohl R, Wilsdorf E (1966) Der Leisniger Quarzporphyr des nordsächsischen Porphyrgebietes und seine Verwitterung. N Jb Geol Paläont, Monatshefte, 4–13
- Kempe U, Götze J, Belyatsky BV, Plötze M (1997) Ce anomalies in monazite, fluorite and agate from Permian volcanics of the Saxothuringian (Germany). J Czech Geol Soc 42(3):38
- Mashkovtsev RI, Shcherbakova MYa, Solntsev VP (1978) EPR of radiation hole centers in a-quartz. Trudy Instituta Geologii I Geofyziki Akademii Nauk SSSR, Sib Otd (Novosibirsk: Nauka) 385:78–86 (in Russian)
- Monecke T, Bombach G, KlemmW KU, Götze J, Wolf D (2000) Determination of trace elements in quartz standard UNS-SpS and in natural quartz by ICP-MS. Geostand Newslett 24(1):73–81
- Moore DM, Reynolds RC Jr (1997) X-ray diffraction and the identification and analysis of clay minerals, 2nd edn. Oxford University Press, Oxford
- Müller A, Wiedenbeck M, Flem B, Schiellerup H (2008) Refinement of phosphorus determination in quartz by LA-ICP-MS through defining new reference material values. Geostand Geoanal Res 32:361–376
- Müller A, van den Kerkhof AM, Behr HJ, Kronz A, Koch-Müller M (2010)
  The evolution of late-Hercynian granites and rhyolites documented
  by quartz a review. Geol Soc Amer Special Papers 472:185–204
- Neuser RD, Bruhn F, Götze J, Habermann D, Richter DK (1995) Kathodolumineszenz: Methodik und Anwendung. Zentralbl Geol Paläontol I, H 1(2):287–306
- Nilges MJ, Pan Y, Mashkovtsev RI (2008) Radiation-induced defects in quartz. I. Single-crystal W-band EPR study of an electron irradiated quartz. Phys Chem Minerals 35:103–115

Ortoleva P, Chen Y, Chen W (1994) Agates, geodes, concretions and orbicules: self-organized zoning and morphology. In: Fractals and Dynamic Systems in Geosciences, 283–305

- Pan Y, Nilges MJ, Mashkovtsev RI (2008) Radiation-induced defects in quartz. II. Single-crystal W-band EPR study of natural citrine quartz. Phys Chem Minerals 35:387–397
- Pan Y, Li D, Feng R, Wiens E, Chen N, Götze J, Lin J (2021) Uranyl binding mechanism in microcrystalline silicas: A potential missing link for uranium mineralization by direct uranyl co-precipitation and environmental implications. Geochim Cosmochim Acta 292:518–531
- Pietzsch K (1962) Geologie von Sachsen. VEB Deutscher Verlag der Wissenschaften, Berlin, p 870
- Powolny T, Dumańska-Słowik M, Sikorska-Jaworowska M, Wójcik-Bania M (2019) Agate mineralization in spilitized Permian volcanics from "Borówno" quarry (Lower Silesia, Poland) microtextural, mineralogical, and geochemical constraints. Ore Geology Reviews 114:103130
- Rehda J (2018) Physical volcanology and petrography of the Lower Permian Leisnig Quartz Porphyry (North Saxon Volcanic Complex). Master thesis, TU Bergakademie Freiberg, Germany, 93 pp
- Repstock A, Breitkreuz C, Lapp M, Schulz B (2018) Voluminous and crystal-rich igneous rocks of the Permian Wurzen volcanic system, northern Saxony, Germany: physical volcanology and geochemical characterization. International J Earth Sci 107:1485–1513
- Röllig G (1976) Zur Petrogenese und Vulkanotektonik der Pyroxenquarzporphyre (Ignimbrite) des Nordsächsischen Vulkanitkomplexes. Jb Geol 5(6):175–268
- Röllig G, Eigenfeld F, Fischer I, Kuhn B (1970) Die Ignimbrite des Nordwestsächsischen Vulkanitkomplexes. Wiss Z MLU Halle-Wittenberg. Math Naturwiss Reihe 19:67–78
- Rykart R (1995) Quarz-Monographie. Ott Verlag, Thun, p 462
- Schwerdtner G, Anger H, Störr M (2007) Die Kaolinlagerstätten des Kemmlitzer Reviers. Bergbaumonographie, Freiberg, 116 pp
- Siegel G, Marrone MJ (1981) Photoluminescence in as-drawn and irradiated silica optical fibers: An assessment of the role of nonbridging oxygen defect centres. J Non-Cryst Solids 45:235–247
- SivaRamiah G, Lin J, Pan Y (2011) Electron paramagnetic resonance spectroscopy of Fe<sup>3+</sup> ions in amethyst: thermodynamic potentials and magnetic susceptibility. Phys Chem Minerals 38:159–167
- Stevens-Kalceff MA (2009) Cathodoluminescence microcharacterization of point defects in α-quartz. Mineral Mag 73:585–606
- Taut T, Kleeberg R, Bergmann J (1998) Seifert software: the new Seifert Rietveld program BGMN and its application to quantitative phase analysis. Mater Struct 5(1):57–66
- Walter H, Grimmer A, Krentz O (1996) Sucharbeiten Auf Quarzporphyrkaoline in Nordwestsachsen Geoprofil 6:115–128
- Walter H (2012) Rotliegend im Nordwestsächsischen Becken. Schriftenreihe Dt Ges Geowiss 61:517–529
- Wang Y, Merino E (1990) Self-organizational origin of agates: banding, fiber twisting, composition, and dynamic crystallization-model. Geochim Cosmochim Acta 54:1627–1638
- Wendt I, Höhndorf A, Wendt JI, Müller P, Wetzel K (1995) Radiometric dating of volcanic rocks in NW-Saxony by combined use of U-Pb and Sm-Nd zircon dating as well as Sm-Nd and Rb-Sr whole-rock and mineral systematics. Terra Nostra 7:147–148
- Wetzel K, Gerstenberger H, Wand U, Wendt I (1995) Zur Geochemie der nordwestsächsischen Vulkanite. Z Geol Wiss 23(4):371–400
- Winchester J, Floyd PA (1977) Geochemical discrimination of different magma series and their differentiation products using immobile elements. Chem Geol 20:325–343
- Wood SA (1990) The aqueous geochemistry of the rare-earth elements and yttrium. 2. Theoretical predictions of speciation in hydrothermal solutions to 350 °C at saturation water vapor pressure. Chem Geol 88:99–125

**Publisher's Note** Springer Nature remains neutral with regard to jurisdictional claims in published maps and institutional affiliations.